

## Tubulin hyperacetylation in *Trypanosoma cruzi*

# Alpha-tubulin acetylation in *Trypanosoma cruzi*: a dynamic instability of microtubules is required for replication and cell cycle progression

1 Victoria Lucia Alonso<sup>1,2</sup>, Mara Emilia Carloni<sup>2†</sup>, Camila Silva Gonçalves<sup>3,4</sup>, Gonzalo Martinez  
2 Peralta<sup>1,2</sup>, Maria Eugenia Chesta<sup>5</sup>, Alejandro Pezza<sup>1</sup>, Luis Emilio Tavernelli<sup>1</sup>, Maria Cristina  
3 M. Motta<sup>3,4\*</sup> and Esteban Serra<sup>1,2\*</sup>

4 <sup>1</sup>Laboratorio de Biología y Bioquímica de *Trypanosoma cruzi*, Instituto de Biología Molecular y  
5 Celular de Rosario (IBR), Consejo Nacional de Investigaciones Científicas y Técnicas (CONICET),  
6 Rosario, Argentina.

7 <sup>2</sup>Facultad de Ciencias Bioquímicas y Farmacéuticas, Universidad Nacional de Rosario (UNR),  
8 Rosario, Argentina.

9 <sup>3</sup>Laboratório de Ultraestrutura Celular Hertha Meyer, Instituto de Biofísica Carlos Chagas Filho,  
10 Universidade Federal do Rio de Janeiro, Rio de Janeiro, Brazil.

11 <sup>4</sup>Instituto Nacional de Ciência e Tecnologia em Biologia Estrutural e Bioimagens, Rio de Janeiro,  
12 Brazil.

13 <sup>5</sup>Facultad de Ciencias Médicas, Universidad Nacional de Rosario (UNR), Rosario, Argentina.

### 14 \* Correspondence:

15 Esteban Serra (serra@ibr-conicet.gov.ar) and Maria Cristina M. Motta (motta@biof.ufrj.br)

16 <sup>†</sup>Current address: Yersinia Research Unit, Institut Pasteur, Microbiology Department, Paris, France.

### 17 **Keywords:** Tubulin, Cytoskeleton, Flagella, Acetylation, Cell division

### 18 **Abstract**

19 Trypanosomatids have a cytoskeleton arrangement that is simpler than what is found in most  
20 eukaryotic cells. However, it is precisely organized and constituted by stable microtubules. Such  
21 microtubules compose the mitotic spindle during mitosis, the basal body, the flagellar axoneme and  
22 the subpellicular microtubules, which are connected to each other and also to the plasma membrane  
23 forming a helical arrangement along the central axis of the parasite cell body. Subpellicular, mitotic  
24 and axonemal microtubules are extensively acetylated in *Trypanosoma cruzi*. Acetylation on lysine  
25 (K) 40 of  $\alpha$ -tubulin is conserved from lower eukaryotes to mammals and is associated with  
26 microtubule stability. It is also known that K40 acetylation occurs significantly on flagella,  
27 centrioles, cilia, basal body and the mitotic spindle in eukaryotes. Several tubulin posttranslational  
28 modifications, including acetylation of K40, have been catalogued in trypanosomatids, but the  
29 functional importance of these modifications for microtubule dynamics and parasite biology remains  
30 largely undefined. The primary tubulin acetyltransferase that delivers this modification was recently  
31 identified in several eukaryotes as Mec-17/ATAT, a Gcn5-related N-acetyltransferase. Here, we  
32 report that *T. cruzi* ATAT acetylates  $\alpha$ -tubulin *in vivo* and is capable of auto-acetylation. *TcATAT* is  
33 located in the cytoskeleton and flagella of epimastigotes and colocalizes with acetylated  $\alpha$ -tubulin in  
34 these structures. We have expressed *TcATAT* with an HA tag using the inducible vector p*TcINDEX*-  
35 GW in *T. cruzi*. Over-expression of *TcATAT* causes increased levels of the acetylated isoform,  
36 induces morphological and ultrastructural defects, especially in the mitochondrion, and causes a halt  
37 in the cell cycle progression of epimastigotes, which is related to an impairment of the kinetoplast  
38 division. Finally, as a result of *TcATAT* over-expression we observed that parasites became more

## Tubulin hyperacetylation effect in *Trypanosoma cruzi*

39 resistant to microtubule depolymerizing drugs. These results support the idea that  $\alpha$ -tubulin  
40 acetylation levels are finely regulated for the normal progression of *T. cruzi* cell cycle.

### 41 1. Introduction

42 *Trypanosoma cruzi*, the etiological agent of Chagas disease or American trypanosomiasis, is a  
43 kinetoplastid parasite with a complex life cycle that alternates between a mammalian host and an  
44 insect host (Triatominae family), which is the biological vector of this disease. The World Health  
45 Organization classifies Chagas disease as one of the 13 most neglected tropical diseases, constituting  
46 a very important social and economic problem in Latin America (WHO, 2012; <http://who.int>).  
47 Trypanosomatids have a cytoskeleton arrangement that is simpler than what is found in most  
48 eukaryotic cells. However, it is precisely organized and constituted by stable microtubules (MT).  
49 Such MTs are present in the mitotic spindle during mitosis, the basal body, the flagellar axoneme and  
50 the subpellicular MTs, which are connected to each other and also to the plasma membrane, thus  
51 forming a helical arrangement along the central axis of the parasite cell body (Vidal et al., 2017).  
52 MTs provide the basis for cytoskeletal architecture and are formed by  $\alpha/\beta$ -tubulin heterodimers,  
53 comprising 13 typical protofilaments connected to each other forming helical tubes. These structures  
54 are regulated by interacting with a variety of MT-associated proteins (MAPs), also by a differential  
55 expression of  $\alpha$  and  $\beta$ -tubulin genes (tubulin isotypes) and by a plethora of post-translational  
56 modifications (PTMs) (Gadadhar et al., 2017). Several conserved lysines in  $\alpha$ - and  $\beta$ -tubulin are  
57 acetylated in eukaryotes, and acetylation of the  $\alpha$ -tubulin luminal residue lysine 40 (K40) has been  
58 the most characterized since its discovery over thirty years ago (L'Hernault and Rosenbaum, 1985;  
59 Al-Bassam and Corbett, 2012; Kull and Sloboda, 2014; Eshun-Wilson et al., 2019). Acetylation of  $\alpha$ -  
60 tubulin on K40 was associated with the stability of microtubules and described as a marker of  
61 microtubules resistance to depolymerizing drugs from the beginning of its study (L'Hernault and  
62 Rosenbaum, 1985; Piperno et al., 1987). In most cells acetylated  $\alpha$ -tubulin is a minor isoform,  
63 observed in primary cilia, flagella, centrioles and neuronal axons (Piperno et al., 1987; Hubbert et al.,  
64 2002; Kalebic et al., 2012; Nakakura et al., 2015). In contrast, trypanosomatids have a significantly  
65 high proportion of acetylated  $\alpha$ -tubulin, concentrated in the subpellicular, mitotic and axonemal MTs  
66 (Sasse and Gull, 1988; Souto-Padron et al., 1993), which makes these organisms attractive models to  
67 study the function of  $\alpha$ -tubulin K40 acetylation.

68 Although acetylation typically correlates with stable and long-lived microtubules in cells, acetylation  
69 itself does not confer stability, but may rather make microtubules more resilient to mechanical forces  
70 (Howes et al., 2013; Szyk et al., 2014; Coombes et al., 2016; Portran et al., 2017). Yet despite years  
71 of study, the effects of acetylation on MTs and MT function in cells are still debated. The primary  $\alpha$ -  
72 tubulin acetyltransferase that delivers this modification was recently identified in several eukaryotes  
73 as MEC-17/ATAT, a Gcn5-related N-acetyltransferase containing a catalytic domain that is  
74 conserved from protists to mammalian species. MEC-17/ATAT directly promotes  $\alpha$ -tubulin  
75 acetylation *in vitro* and it is the major  $\alpha$ -tubulin acetyltransferase *in vivo* (Akella et al., 2010; Shida et  
76 al., 2010). MEC-17 is required for touch sensation in *Caenorhabditis elegans*, normal embryonic  
77 development in zebrafish, and the rapid assembly of primary cilia in RPE-hTERT cells (Akella et al.,  
78 2010; Shida et al., 2010; Li et al., 2012). Also, acetylation does not seem to be only a passive mark  
79 on microtubules, as its loss disrupts microtubule structural integrity in touch receptor neurons,  
80 leading to axonal morphology defects (Cueva et al., 2012). Loss of ATAT also causes brain  
81 abnormalities in mice (Kim et al., 2013). ATAT was characterized in the apicomplexan parasite  
82 *Toxoplasma gondii* where it was shown that K40 acetylation stabilizes MTs and is required for  
83 replication. *TgATAT* is expressed in a cell cycle-regulated manner and genetic disruption ablates  
84 K40 acetylation, thus inducing replication defects, since parasites appear to initiate mitosis but  
85 exhibit an incomplete or improper nuclear division (Varberg et al., 2015).

## Tubulin hyperacetylation in *Trypanosoma cruzi*

Several tubulin PTMs, including acetylation of K40, have been catalogued in trypanosomatids (Rosenzweig et al., 2008; Nett et al., 2009; Tsigankov et al., 2013; Moretti et al., 2018), but the functional importance of these modifications for MT dynamics and parasite biology remains largely undefined. We have studied the effect of  $\alpha$ -tubulin hyperacetylation on *T. cruzi* cell cycle by over-expressing its  $\alpha$ -tubulin acetyltransferase (*TcATAT*) using the tetracycline-inducible vector *pTcINDEX-GW* (Alonso et al., 2014a). This system allowed us to control the amount of *TcATAT*, and hence the amount of acetylated  $\alpha$ -tubulin in epimastigotes. Over-expressing parasites showed an increase of acetylated  $\alpha$ -tubulin as expected that was associated to growth defects related to a cell cycle arrest and impairment of kinetoplast division. *TcATAT* is located in the cytoskeleton and flagella of *T. cruzi* and colocalizes with acetylated  $\alpha$ -tubulin. Over-expression also induced morphological alterations, that are related to cell division impairment, and ultrastructural changes, especially in the mitochondrial branches and in kDNA topology. These evidence supports the idea that  $\alpha$ -tubulin acetylation is tightly regulated in *T. cruzi* and indicates that although the cytoskeleton arrangement is considered stable in trypanosomatids, a dynamic instability of microtubules is required for replication and cell cycle progression.

## 2. Materials and Methods

### 2.1. Molecular cloning of *TcATAT-HA*

*TcATAT* gene from *T. cruzi* Dm28c strain were amplified using the following oligonucleotides, TATFw: AAGGATTCATGTATCCGTATGATGTCCCGATTATGCTAGTTCCACATCGCAA and TATRv: AACTCGAGTGTTCTGGAGTACCACT, adding and HA-tag in the N-terminus (in bold). DNA purified from *T. cruzi* Dm28c epimastigotes was used as template. The PCR products obtained with a proofreading DNA polymerase were inserted into pCR2.1-TOPO vector (Invitrogen) and sequenced. *TcATAT-HA* coding regions was then inserted into a pENTR3C vector (Gateway system Invitrogen) using the *Bam*HI/*Xho*I restriction sites included in the oligonucleotides (underlined) and then transferred to pDEST17 (Gateway system Invitrogen) and *pTcINDEX-GW* vectors by recombination using LR clonase II enzyme mix (Invitrogen). The pDEST17 constructs were transformed into *Escherichia coli* BL21 pLysS and recombinant proteins, fused to a six histidine-tag, were obtained by expression-induction with 0.5 mM IPTG for 3 h at 30°C. The proteins were purified by affinity chromatography using a Ni-NTA agarose resin (Qiagen) following the manufacturer's instructions.

### 2.2. *Trypanosoma cruzi* culture and transfection

*T. cruzi* Dm28c epimastigotes were cultured at 28 °C in LIT medium (5 g/L liver infusion, 5 g/L bacto-tryptose, 68 mM NaCl, 5.3 mM KCl, 22 mM Na2HPO4, 0.2% (w/v) glucose and 0.002% (w/v) hemin) supplemented with 10% (v/v) heat-inactivated, UV-irradiated Fetal Calf Serum (FCS) (Internegocios S.A, Argentina). Viability was determined by counting live cells with a haematocytometer using Erythrosin B staining. For half media inhibitory concentration (IC<sub>50</sub>) calculations parasites were treated with Oryzalin (0-300  $\mu$ M) for 72 h. and the number of parasites was plotted against the log[Oryzalin]. The plot was fitted with the non-parametric regression log(inhibitor) vs. response -Variable slope (four parameters) in GraphPad Prism version 8.0. Epimastigotes' motility was examined using the computer-assisted semen analysis (CASA) system (Microptic, SCA evolution). Parameters used were as follows: 30 frames acquired, frame rate of 60 Hz, and cell size of 10–100  $\mu$ m<sup>2</sup>. At least 30 microscopy fields corresponding to a minimum of 300 epimastigotes were analyzed in each experiment.

## Tubulin hyperacetylation effect in *Trypanosoma cruzi*

129 Epimastigotes from *T. cruzi* Dm28c were transfected with the pLEW13 plasmid to generate parasites  
130 expressing T7 RNA polymerase and the tetracycline repressor using a nucleofection method. Briefly,  
131 epimastigotes were cultured in LIT medium at 28 °C to a final concentration of 4x10<sup>7</sup> parasites per  
132 transfection. Then, parasites were harvested by centrifugation at 1500 g for 10 min at room  
133 temperature, washed once with phosphate buffered saline (PBS) and resuspended in 0.4 mL BSF  
134 transfection buffer (5 mM KCl, 0.15 mM CaCl<sub>2</sub> 90 mM, Na<sub>2</sub>HPO<sub>4</sub> 50 mM HEPES pH 7.3).  
135 Nucleofection (Nucleofector 2B, Lonza) was performed in a 0.2 cm gap cuvette (Bio-Rad) with ~20  
136 µg of plasmid DNA added to a final volume of 400 µL. The parasite-DNA mixture was kept on ice  
137 for 20 min prior to nucleofection with program X-014. After nucleofection, cells were transferred  
138 into 3 mL of LIT medium containing 20% FCS, maintained at room temperature for 15 minutes and  
139 then incubated at 28 °C. Geneticin (G418; Life Technologies) was added at a concentration of 200  
140 µg/mL, and parasites were incubated at 28 °C. After selection, pLEW13 transfected epimastigotes  
141 were maintained in the presence of 100 µg/ml of G418 (Sigma Aldrich). This parental cell line was  
142 then nucleofected with pTcINDEX-GW *Tc*ATAT-HA construct following a similar protocol and  
143 transgenic parasites were obtained after 4 weeks of selection with 100 µg/ml G418 and 200 µg/ml  
144 Hygromycin B (Sigma Aldrich).

### 145 2.3. Polyclonal antibodies

146 All experiments were approved by the Institutional Animal Care and Use Committee of the School of  
147 Biochemical and Pharmaceutical Sciences, National University of Rosario (Argentina) (File  
148 6060/227) and conducted according to specifications of the US National Institutes of Health  
149 guidelines for the care and use of laboratory animals. Rabbits were only used for the production of  
150 polyclonal antibodies. A rabbit was immunized two times with recombinant ATAT-HA protein  
151 purified from *E. coli* and an equal volume of Freund's adjuvant. The animal was bled two weeks after  
152 the final injection.

### 153 2.4. Protein extracts

154 Exponentially growing epimastigotes were washed twice with cold PBS, and the pellets were  
155 resuspended in lysis buffer (20 mM HEPES, 8 M Urea) and incubated for 30 min at room  
156 temperature with gentle agitation. Insoluble debris was eliminated by centrifugation. The same  
157 procedure was applied to amastigote and trypomastigote cellular pellets. *T. cruzi* cytoskeleton-  
158 enriched extracts were prepared as previously described (Alonso et al., 2014b).  
159

### 160 2.5. Western blot

161 Protein extracts were fractioned in SDS-PAGE and transferred to a nitrocellulose membrane.  
162 Transferred proteins were visualized with Ponceau S staining. Membranes were treated with 10%  
163 non-fat milk in PBS for 2 hours and then incubated with specific antibodies diluted in 0.5% Tween  
164 20 in PBS (PBS-T) for 3 hours. Primary antibodies used were: rat monoclonal anti-HA 1:2000  
165 (ROCHE), affinity-purified rabbit polyclonal anti-*Tc*ATAT 1:200, mouse monoclonal anti-  
166 trypanosome α-tubulin clone TAT-1 1:1000 (a gift from K. Gull, University of Oxford, UK), rabbit  
167 polyclonal anti-Acetyl-lysine 1:1000 (Millipore), mouse monoclonal anti-acetylated α-tubulin clone  
168 6-11B-1 1:2000 (Sigma Aldrich). Bound antibodies were detected using peroxidase-labeled anti-  
169 rabbit IgG (GE Healthcare), anti-mouse IgG (GE Healthcare) or anti-rat IgG (Thermo Scientific) and  
170 developed using ECL Plus kit (GE Healthcare) according to manufacturer's protocols.  
171 Immunoreactive bands were visualized and photographed in the Amersham Imager 600 (GE  
172 Healthcare). Images were processed and bands were quantified with ImageJ (Miller, 2010).

## Tubulin hyperacetylation in *Trypanosoma cruzi*

### 173 2.6. Preparation of cytoskeletal and flagellar complexes

174 The isolated cytoskeletons and flagellar complexes were obtained as previously described (Alonso et  
175 al., 2016) and followed by the immunofluorescence protocol as described below.

### 176 2.7. Immunofluorescence

177 Trypomastigotes and exponentially growing epimastigotes were centrifuged, washed twice in PBS,  
178 settled on polylysine-coated (Sigma Aldrich) coverslips and fixed with 4% para-formaldehyde in PBS  
179 at room temperature for 20 minutes. For the mitochondrial staining, epimastigotes were resuspended  
180 in PBS and incubated with 1  $\mu$ M MitoTracker Orange CMTMRos (Invitrogen) for 30 minutes at  
181 28°C, washed twice in PBS and fixed with 4% para-formaldehyde. Fixed parasites were washed with  
182 PBS and permeabilized with 0.1% Triton X-100 in PBS for 10 minutes. After washing with PBS,  
183 parasites were incubated with the appropriate primary antibody diluted in 5% BSA in PBS for 2  
184 hours at room temperature. Primary antibodies used were: rat monoclonal anti-HA 1:200 (ROCHE),  
185 affinity-purified rabbit polyclonal anti-*Tc*ATAT 1:20, mouse monoclonal anti-acetylated  $\alpha$ -tubulin  
186 clone 6-11B-1 1:100 (Sigma Aldrich) and mouse polyclonal anti-PAR2 1:100 (*T. cruzi* paraflagellar  
187 rod 2 protein). In colocalization experiments both antibodies were incubated together. Non-bound  
188 antibodies were washed with 0.01% Tween 20 in PBS and then the slides were incubated with  
189 fluorescent-conjugated anti-mouse Alexa-555 (Invitrogen) or anti-rat (FITC, Invitrogen) and anti-  
190 rabbit (FITC, Jackson Immuno Research) IgG antibodies and 2  $\mu$ g/mL of DAPI for 1 hour. The slides  
191 were washed with 0.01% Tween 20 in PBS and finally mounted with VectaShield (Vector  
192 Laboratories). Images were acquired with a confocal Zeiss LSM880 and Nikon Eclipse Ni-U  
193 epifluorescence microscope. ImageJ software were used to process all images.

### 194 2.8. Ultrastructural analysis

#### 195 2.8.1. Scanning electron microscopy (SEM)

196 Cells were fixed in 2.5% glutaraldehyde diluted in 0.1 M cacodylate buffer (pH 7.2) for 1 h,  
197 following washes in the same buffer and then adhered to poly-L-lysine-coated microscope coverslips.  
198 After fixation, parasites were post-fixed with 1% osmium tetroxide diluted in cacodylate buffer for 1  
199 hour, dehydrated in ethanol (50%, 70%, 90%, and two exchanges of 100%, 10 min in each step),  
200 critical point dried in CO<sub>2</sub> by using a Leica EM CPD030 equipment (Leica, Wetzlar, Germany) and  
201 ion sputtered in a Balzers FL9496 unit (Postfach 1000 FL-9496 Balzers Liechtenstein). Samples were  
202 observed under an EVO 40 VP SEM (Zeiss, Germany).

#### 203 2.8.2. Transmission electron microscopy (TEM)

204 Cells were fixed as described for Scanning electron microscopy. Then, samples were post-fixed in  
205 1% osmium tetroxide and 0.8% potassium ferricyanide, diluted in the same buffer, for 1 h. After this,  
206 parasites were washed in cacodylate buffer, dehydrated in a graded series of acetone (50%, 70%,  
207 90%, and two exchanges of 100%, 10 min in each step) and embedded in Polybed resin (Epon)  
208 (Electron Microscopy Sciences, Hatfield, PA, USA). Ultra-thin sections were stained with uranyl  
209 acetate for 40 min and then with lead citrate for 5 min. Samples were observed under a Jeol 1200 EX  
210 TEM operating at 80 kV (Jeol, Japan).

### 211 2.9. Cell Cycle analysis

212 Synchronization of epimastigotes in G1 of the cell cycle was achieved using hydroxyurea (HU).  
213 Cells in exponential growth phase were arrested by incubation with 20 mM of HU for 24 h and then  
214 released by washing twice with PBS and suspending the cells in culture medium. Cells continued to

## Tubulin hyperacetylation effect in *Trypanosoma cruzi*

215 be cultured for 24 h and samples were taken at the indicated time points. Cell cycle progression of  
216 parasites was analyzed by flow cytometry as described previously (Tavernelli et al., 2019). Briefly,  
217 one million cells were fixed with cold 70% ethanol and then washed with PBS and stained with 20  
218 µg/ml Propidium Iodide (PI) in buffer K (0.1% sodium citrate, 0.02 mg/mL RNase A (Sigma), and  
219 0.3% NP-40). Ten thousand events per sample were acquired using BD Cell Sorter BD FACSAria II.  
220 Results were analyzed with FlowJo software.

### 221 2.10. ATAT-HA purification form *T. cruzi* epimastigotes

222 A culture of 50 ml of *T. cruzi* Dm28c pTcINDEX-GW-ATAT-HA induced with 0.5 µg/mL  
223 tetracycline for 24 hours was collected and resuspended in 500 µL lysis buffer MME (Mops pH 6,9  
224 10 mM, EGTA-EDTA 1 mM, MgSO<sub>4</sub> 1 mM) supplemented with NaCl 1M, Triton X-100 0.2% and  
225 protease inhibitor cocktail (GE). Incubated with agitation at 4°C for 30 min and then cells were  
226 ruptured by sonication and centrifuged for 20 min. at 16,000 g. The supernatant was loaded to an  
227 anti-HA agarose column (Roche) following the manufacturers' instructions. The flowthrough was  
228 collected, and the column was washed with 1 volume of PBS 0.5% Tween-20. The bound protein  
229 was eluted four times with 250 µL of HA peptide (Sigma-Aldrich) (0,1 mg/ml).

### 230 2.11. Autoacetylation assay

231 0.5 µg of ATAT-HA purified from *T. cruzi* epimastigotes was incubated in the absence or presence  
232 of 0.5 mM Acetyl CoA (Sigma) for 1.5 h at 37°C in acetylation buffer (50mM Tris-HCl, pH 8.0;  
233 10% glycerol; 1mM MgCl<sub>2</sub>; 1mM DTT; 1mM PMSF; 20mM sodium butyrate). The samples were  
234 resolved on SDS-PAGE gels, transferred to nitrocellulose membranes (GE Healthcare) and subjected  
235 to western blot analysis as described above.

## 236 3. Results

### 237 3.1. ATAT homologue in *T. cruzi* is expressed in all *T. cruzi* life cycle stages

238 A bioinformatic survey of the *T. cruzi* genome in TriTrypDB (<https://tritrypdb.org/>) revealed a single  
239 gene containing a MEC-17 domain belonging to the Gcn5-related superfamily (PF05301), described  
240 in this database as a putative alpha-tubulin N-acetyltransferase. In the genome of the Dm28c strain  
241 the predicted protein sequence is 330 amino-acids long with the acetyltransferase domain in its N-  
242 terminal portion (C4B63\_12g332), from now on we will name it *TcATAT* (Figure 1). When we  
243 looked for homologs in other trypanosomatids, we found that the in *T. brucei* (Tb927.3.1400) the  
244 putative alpha-tubulin N-acetyltransferase contains 55% of identical residues compared to *T. cruzi*  
245 and that this homology is widespread along the sequence. In the case of *Leishmania mayor*  
246 (LmjF.25.1150) the identity is restricted to the acetyltransferase domain (50% identical residues)  
247 (Supplementary Figure S1A). When we aligned the acetyltransferase domains of ATAT homologues  
248 from several representative species with Clustal Omega, we observed that the acetyltransferase  
249 domain is highly conserved, including the key residues critical for the enzymatic activity (asterisks in  
250 Figure 1B), while both N-terminal and C-terminal portions of the different homologs are highly  
251 dissimilar and even have different lengths (Figure 1A). For example, the *Toxoplasma gondii* ATAT  
252 is considerably larger than all previously characterized ATAT/MEC-17 proteins (Varberg et al.,  
253 2015).

254 RNAseq experiments showed that *TcATAT* transcripts are more abundant in trypomastigote stage  
255 compared to epimastigote stage (Smircich et al. 2015) and that they peak in late amastigote and  
256 trypomastigote stages (Li et al., 2016). To assess the expression pattern of *TcATAT* in all the three  
257 stages of *T. cruzi* life cycle we obtained polyclonal antibodies from rabbit against the recombinant

## Tubulin hyperacetylation in *Trypanosoma cruzi*

258 protein that were purified and used in western blot and immunofluorescence assays in epimastigotes,  
259 amastigotes and trypomastigotes. We observed that *TcATAT* is expressed in all life cycle stages,  
260 located in the whole cell body of *T. cruzi* and apparently excluded from the nuclei (Figure 1C). Some  
261 discrete spots in the perinuclear area in epimastigotes and amastigotes were also observed (Figure  
262 1C, white arrowheads). As expected, we detected *TcATAT* by western blot in whole extracts of  
263 epimastigotes, trypomastigotes and amastigotes, with a higher expression in the last stage (Figure  
264 1D).

### 265 3.2. *TcATAT-HA* has acetyltransferase activity and acetylates $\alpha$ -tubulin in the cytoskeleton 266 and flagellum of epimastigotes

267 To determine the impact of *TcATAT* on  $\alpha$ -tubulin acetylation we obtained *T. cruzi* epimastigotes  
268 stably transfected with the p*TcINDEX-GW* vector (Alonso et al., 2014a) baring the ATAT coding  
269 sequence with a hemagglutinin tag on its N-terminus (HA). This plasmid allowed us to induce the  
270 expression of the transgene with tetracycline (Taylor and Kelly, 2006). We corroborated the over-  
271 expression of *TcATAT-HA* in epimastigotes by immunofluorescence and western blot assays with  
272 anti-HA antibodies 24 h post-induction (p.i.) (Figure 2A and 2B), and we did not detect tagged  
273 protein without tetracycline induction (Figure 2B and Supplementary Figure S2). At this time, an  
274 evident phenotypic defect was detected in the induced parasites (Figure 2A, arrowhead) and a round  
275 refringent structure was observed in a proportion of the over-expressing epimastigotes.

276 Then, we quantified the amount of acetylated  $\alpha$ -tubulin at different induction times by densitometry  
277 (Figure 2C) in the over-expressing epimastigotes. The amount of acetylated  $\alpha$ -tubulin increased with  
278 *TcATAT-HA* induction time being almost 10 times higher at 24 h.p.i. compared to the uninduced  
279 control. ATAT shows autoacetylation activity in other organisms (Kalebic et al., 2012; Zhou et al.,  
280 2018) and *TcATAT* was predicted to be acetylated on K263 with the PAIL server (Deng et al., 2016).  
281 To study if this was also the case for *T. cruzi* we performed an autoacetylation assay using purified  
282 *TcATAT-HA* from epimastigotes incubated in the absence or presence of Acetyl-CoA. We detected  
283 acetylated *TcATAT* only in the presence of Acetyl-CoA confirming that *TcATAT* has a fully  
284 functional domain with acetyltransferase activity (Figure 2D).

285 We also tested whether ATAT-HA overexpressing epimastigotes were more resistant to the  
286 microtubule-disrupting drug Oryzalin to correlate acetylation with stability. Oryzalin effect on *T. cruzi*  
287 has not been reported yet, but we found in the literature that a similar dinitroaniline, Trifuralin, had an  
288 IC<sub>50</sub> between 70 and 160  $\mu$ M depending on the strain used (Traub-Cseko et al., 2002). To begin with,  
289 we determined Oryzalin IC<sub>50</sub> in Dm28c epimastigotes (250.5  $\mu$ M) and found that it was higher than  
290 what was reported for Trifuralin (Supplementary Figure S3A). Epimastigotes treated with Oryzalin  
291 show a dose-dependent loss of normal morphology: at higher concentrations epimastigotes adopt a  
292 rounded shape with a shorter flagellum - perhaps due to alterations in the polymerization of axonemal  
293 microtubules (Supplementary Figure S3B). In presence of 200  $\mu$ M Oryzalin, Dm28c p*TcINDEX-GW*  
294 ATAT-HA epimastigotes induced with tetracycline grew better than uninduced parasites (Table I), as  
295 expected for an increased amount of acetylated  $\alpha$ -tubulin.

296 To better characterize the localization of *TcATAT*, we isolated subpellicular microtubules and flagellar  
297 complexes from transfected epimastigotes and analyzed the presence of *TcATAT-HA* in these  
298 structures. As observed in Figure 3A, ATAT-HA colocalizes with acetylated  $\alpha$ -tubulin in the  
299 subpellicular microtubules and the flagellar axoneme. The round structured observed by light  
300 microscopy remains insoluble after treatment with detergent and NaCl and is labeled with the anti-  
301 HA/FITC antibody. When the confocal images of these preparations are not over-exposed (necessary  
302 to observe the cytoskeletal labelling, which is weaker than in the round structure) it appears that ATAT-  
303 HA is surrounding this structure (Supplementary Figure S4A). In intact epimastigotes fixed with para-  
304 formaldehyde confocal microscopy *TcATAT-HA* was observed as accumulated in the periphery of

## Tubulin hyperacetylation effect in *Trypanosoma cruzi*

305 these round structures (Figure 2A). We performed a Z-stack confocal imaging and 3D reconstruction  
306 (Supplementary movie V1) and observed that *TcATAT-HA* formed a ball-like structure near the  
307 nucleus and the kinetoplast. Furthermore, when we compare cytoskeletal preparations of epimastigotes  
308 uninduced and induced with tetracycline we observed a disruption of the acetylated MTs upon ATAT-  
309 HA over-expression (Supplementary Figure S4B). As a control we verified that *TcATAT-HA* did not  
310 co-localize with the paraflagellar rod that runs parallel to the axoneme (Supplementary Figure S4C).  
311 Also, we obtained protein extracts enriched in cytoskeletal and flagellar proteins and observed by  
312 western blot that both the endogenous ATAT and the over-expressed version are only present in the  
313 fraction that corresponds to insoluble cytoskeletal and flagellar proteins (P, in figure 3B), confirming  
314 that it is tightly associated to these structures.

315 The refringent button-like structure observed in the over-expressing parasites was quantified and it  
316 was present in approximately 20% of the epimastigotes 48 h.p.i. We also determined that this  
317 structure grew with induction time and was usually observed near the nucleus and the kinetoplast  
318 (Figure 4A). Transmission Electron Microscopy (TEM) analyses revealed that this round structure is  
319 electrodense, not delimited by membrane, and sometimes is seen in continuity with the endoplasmic  
320 reticulum, resembling an inclusion body (Figure 4B). These results correlate with the accumulation  
321 of *TcATAT-HA* observed in association to the isolated cytoskeleton where the structure is seen  
322 connected to the flagellum (Figure 3A).

### 323 3.3. $\alpha$ -Tubulin hyperacetylation causes a halt in the cell cycle progression of epimastigotes

324 We performed growth curves of *TcATAT* over-expressing epimastigotes in the absence and  
325 presences of tetracycline. (Figure 5A). A growth impairment was observed after 48 h.p.i. but no  
326 differences in viability (measured with Erythrocin B staining) were observed along the entire growth  
327 curve (Supplementary Figure S5A). We have previously ruled out any undesired effect of the  
328 tetracycline treatment (Ritagliati et al., 2015a). We also quantified epimastigotes' motility using  
329 CASA software and observed less motile parasites when epimastigotes were induced for 48 h.  
330 (Supplementary Figure S5B). Over-expression was also verified with rabbit polyclonal anti-ATAT  
331 antibodies in 24 and 48 h.p.i cells, when the *TcATAT* labeling was particularly strong and excluded  
332 from the nucleus and kinetoplast (Figure 5B). After 24 h.p.i. parasites that appear to have two nuclei  
333 start to accumulate (Zoom in Figure 5B, yellow arrow heads indicate parasites with an aberrant DNA  
334 content). The cell cycle progression of *TcATAT* overexpressing epimastigotes was analyzed by flow  
335 cytometry with Propidium iodide (PI) staining for 24 h.p.i in synchronized epimastigotes (Figure  
336 6A). As expected, in the absence of tetracycline we observed that the cell cycle progressed normally.  
337 At time point 0 the main peak corresponds to the parasites on G1 phase of the cell cycle (~60% of  
338 the total) that is, parasites with the DNA content corresponding to one nucleus. A second minor peak  
339 represents the parasites in G2/M phase (~30%), which corresponds to epimastigotes with the double  
340 of DNA content, including those on cytokinesis. In the valley between the two peaks are the cells on  
341 S phase (~10%). Then, at time point 6 hours the count of parasites in S phase starts to increase and at  
342 12 hours more than half of the parasites are in G2/M phase. Finally, at 24 hours the parasites return to  
343 G1 phase. When tetracycline is added the peak of cells in S phase doubles at 12 h.p.i. Furthermore,  
344 G2/M peak increased about 20% at 24 h.p.i., suggesting that the *TcATAT* overexpression results in  
345 an arrest of cells that are dividing and cells that have duplicated their DNA (Figure 6B). This halt in  
346 the cell cycle progression was also observed by Scanning Electron Microscopy (Figure 6C). When  
347 parasites are induced with tetracycline for 24 hours, ~30% of the cells have two flagella and it  
348 appears that there is an impairment in the cleavage furrow progression and cytokinesis (white arrows,  
349 Figure 6C g -i) that correlates with the higher proportion of cells in G2/M phase.  
350 As a control, we quantified the population of epimastigotes with two nuclei and one kinetoplast 24  
351 and 48 h.p.i in an asynchronous population. The ordered progression of the cell cycle, in which

## Tubulin hyperacetylation in *Trypanosoma cruzi*

352 kinetoplast segregation precedes nuclear division, allows the identification of three normal states  
353 regarding nuclear/kinetoplast (N/K) content: 1N1K, 1N2K and 2N2K. Under normal conditions,  
354 most epimastigotes in a non-synchronous exponentially growing culture contain one nucleus and one  
355 kinetoplast (1N1K, usually ~80–95%), corresponding to parasites in G1 or S phase of the cell cycle.  
356 A smaller proportion exhibits two kinetoplasts and one nucleus (1N2K ~5%), these correspond to  
357 parasites in G2 phase or the beginning of mitosis. Finally, cells presenting two kinetoplasts and two  
358 nuclei (2N2K ~3%) are those that have completed mitosis and are undergoing cytokinesis or ready to  
359 do so (Elias et al., 2007). Thus, the appearance of cells with abnormal N/K content is indicative of  
360 cell cycle impairment. 20-30% more parasites with 1K/2N are found in over-expressing conditions  
361 than in the uninduced control (Supplementary Figure S7).

### 362 3.4. Over-expression of *TcATAT-HA* alters acetylated $\alpha$ -tubulin distribution and causes 363 modifications on mitochondrion ultrastructure

364 Parasites with over-expression of *TcATAT-HA* presented alterations on acetylated  $\alpha$ -tubulin  
365 distribution observe with anti-acetylated  $\alpha$ -tubulin antibodies. Part of the population accumulates  
366 acetylated  $\alpha$ -tubulin around the kinetoplast (Figure 7A, yellow arrowheads) and in some parasites it  
367 is surrounding the inclusion body-like structure (Figure 7A, white arrowheads).  
368 Trypanosomatids have a single and ramified mitochondrion with the kDNA concentrated in the  
369 kinetoplast. The kinetoplast is connected to the basal body that nucleates the flagellum, that are both  
370 MT-containing structures. Since the basal body is linked to the kinetoplast by the tripartite  
371 attachment complex (TAC) (Kaser et al., 2014), we decided to investigate the mitochondrial  
372 morphology and ultrastructure in *TcATAT-HA* over-expressing cells by TEM and using Mitotracker  
373 Orange CMTMRos. In induced epimastigotes, cristae swelling was seen in the kinetoplast region and  
374 also in the mitochondrial branches (Figure 7B, white arrows in a and b). Moreover, sometimes cells  
375 presented a kinetoplast containing multiple networks that are very condensed (Figure 7B, white  
376 arrow in c) indicating kinetoplast division impairment. Images obtained by TEM confirmed this  
377 hypothesis since overexpressing parasites presented duplicated kDNA that did not suffer scission and  
378 was seen associated to a single basal body (Figure 7C, black arrowheads heads in b), differently to  
379 what was observed in the uninduced condition where cells contained two basal bodies (Figure 7C,  
380 black arrowheads in a). Furthermore, TEM images revealed that when the kDNA duplicated, but the  
381 kinetoplast did not divide, the network became curved, folded over itself, thus acquiring a round  
382 shape with an atypical condensation. The kinetoplast shape also changed from disk to a round format  
383 (Figure 7C, c-f). Such kDNA alterations were also observed by confocal microscopy in *TcATAT-*  
384 *HA* over-expressing parasites stained with Mitotracker and DAPI. Parasites presented a single  
385 kinetoplast with duplicated kDNA and two nuclei (Figure 7D, upper panel), as well an arched kDNA  
386 (Figure 7D, lower panel).

### 387 4. Discussion

388 In this study, we address the biological relevance of acetylated  $\alpha$ -tubulin in the protozoan pathogen  
389 *T. cruzi*. More than 30 years ago it was described that acetylated  $\alpha$ -tubulin was the mayor isotype  
390 present in *T. brucei* (Schneider et al., 1987; Sasse and Gull, 1988) and *T. cruzi* (Souto-Padron et al.,  
391 1993) subpellicular MTs and flagellar axoneme, but the significance of this finding has not been  
392 unraveled yet. We have identified and characterized the acetyltransferase responsible for mediating  
393 K40  $\alpha$ -tubulin acetylation in *T. cruzi*, *TcATAT*, and shown that its over-expression conduced to a  
394 hyperacetylation of  $\alpha$ -tubulin that severely affects the normal progression of the cell cycle in  
395 epimastigotes. ATAT-HA over-expression also confers epimastigotes resistance to Oryzalin, a  
396 depolymerizing drug that targets  $\alpha$ -tubulin. Dinitroaniline herbicides such as oryzalin, which was

## Tubulin hyperacetylation effect in *Trypanosoma cruzi*

397 shown to depolymerize plant cell microtubules (Morejohn et al., 1987), also disrupt the microtubules  
398 of several protozoa including *Tetrahymena* (Stargell et al., 1992) and parasites such as *Leishmania*  
399 spp. (Chan et al., 1991), *Entamoeba* spp. (Makioka et al., 2000), *Cryptosporidium parvum* (Armson  
400 et al., 2002), *Toxoplasma gondii* (Stokkermans et al., 1996), *Angomonas deanei* and *Strigomonas*  
401 *culicis* (Catta-Preta et al., 2015). Interestingly, sensitivity of *T. cruzi* to Orlyzalin is significantly  
402 higher than for other protists where it was studied, what can be explained by the presence of a L at  
403 position 267, instead of a V or I found in *Toxoplasma gondii* (Shaw et al., 2000) and *Tetrahymena*  
404 *thermophila* (Dostál and Libusová, 2014) respectively, among other point mutations found in *T. cruzi*  
405  $\alpha$ -tubulin.

406 Acetylated  $\alpha$ -tubulin has been associated with stable structures in eukaryotic cells, localizing to  
407 primary cilia, midbodies, centrioles and subsets of cytoplasmic microtubules in 3T3 and HeLa cells  
408 (Piperno et al., 1987) and to flagella axonemes, basal bodies and cytoplasmic microtubules radiating  
409 from the basal bodies in *Chlamydomonas reinhardtii* (L'Hernault and Rosenbaum, 1985). In *T.*  
410 *brucei* and *T. cruzi* acetylated  $\alpha$ -tubulin is distributed widely throughout all microtubular arrays  
411 (Sasse and Gull, 1988; Souto-Padron et al., 1993). This post-translational modification appears to  
412 occur during or immediately after microtubule polymerization, and the deacetylation process  
413 correlates with depolymerization (Sasse and Gull, 1988). The fact that we observed a resistance to an  
414  $\alpha$ -tubulin depolymerizing drug when MTs are hyperacetylated suggests that there is a clear link  
415 between acetylation and stabilization in *T. cruzi* as reported in other organisms. Subpellicular  
416 microtubules that compose the trypanosomatid cytoskeleton are quite stable structures, but our results  
417 suggest that a fine regulation in tubulin polymerization/depolymerization is necessary for the correct  
418 progression of the cell cycle and protozoan division.

419 Early electron microscopy revealed distinct subcellular sites from which microtubules appeared to  
420 emanate which were named 'microtubule-organizing centers' in eukaryotes (MTOCs). Since then, the  
421 exact nature of MTOCs has remained unclear. Microtubules have an inherent structural polarity, with  
422 a dynamic plus end and a comparatively stable and slow growing minus end. These characteristics of  
423 microtubule minus ends can be influenced *in vivo* by an association with a MTOC, that can be broadly  
424 defined as sites for microtubule nucleation, stabilization, and/or anchoring (Sanchez and Feldman,  
425 2017). Not much is known about MTOCs in trypanosomatids apart from the fact that subpellicular  
426 microtubules have uniform spacing over the entire parasite, presenting their minus ends oriented  
427 toward the anterior pole of the cell, the region where the single-copy organelles division starts (Wheeler  
428 et al., 2019). Trypanosomes have  $\gamma$ -tubulin and  $\gamma$ -tubulin ring complex proteins, but unfortunately their  
429 localization or interrogation of function has not led to the definition of the sites of individual  
430 microtubule nucleation within the subpellicular array (Zhou and Li, 2015). We observed that ATAT is  
431 concentrated in perinuclear spots in epimastigotes and amastigotes, and that it accumulates mainly in  
432 the anterior region when over-expressed. These results as well as the fact that  $\alpha$ -tubulin acetylation  
433 occurs immediately after microtubules polymerization may suggest that ATAT stabilizes the  
434 microtubules that form the subpellicular corset when they are nucleating in the MTOC.

435 The *T. cruzi* cell cycle is characterized by a coordinated duplication of nuclear and kinetoplast DNA  
436 during the S phase. After kDNA replication, the kinetoplast assumes a more elongated disk shape and  
437 segregates at the beginning of the G2 phase. At this point cells present two basal bodies, both linked  
438 to the kDNA network (Elias et al., 2007). TEM analyses revealed that many cells showed an elongated  
439 kinetoplast, indicating that the kDNA replication occurred, but not the network scission. This is related  
440 to hyperacetylation that also caused a marked halt in G2/M phase of the cell cycle as determined by  
441 flow cytometry. A phenotype related to *TcATAT* over-expression is the impaired ingressoin of the  
442 cleavage furrow, resulting in a defect in cytokinesis, an observation that can be associated to an increase  
443 in the amount of acetylated  $\alpha$ -tubulin (or perhaps to a decrease in the amount of non-acetylated  $\alpha$ -  
444 tubulin available). The blocked cytokinesis resembles the phenotype of *T. brucei* GTPase Arl2 mutants.  
445 Arl2 orthologues in mammals are mitochondrial proteins but in *T. brucei* it appears to be a cytoskeletal

## Tubulin hyperacetylation in *Trypanosoma cruzi*

446 protein. Knockdown and over-expression of *TbArl2* modulate the levels of acetylated  $\alpha$ -tubulin and  
447 inhibits cytokinesis and cleavage furrow progression similar to ATAT-HA over-expression (Price et  
448 al., 2010). Furthermore, in *T. brucei* cytokinesis proceeds from the anterior end to the posterior end,  
449 with the cleavage furrow starting at the distal tip of the new Flagellum Attachment Zone (FAZ) and  
450 proceeding along a fold in the cell. The furrow placement relative to the old and new FAZ guarantees  
451 correct inheritance of the basal body, kinetoplasts, and flagellar pocket complexes, but the nuclei must  
452 be positioned correctly. Finally, the furrow resolves to a single point of connection between the  
453 posterior of one daughter cell and the side of the other daughter. This narrow cytoplasmic bridge can  
454 persist while the daughter cells restart the cell cycle, although it is normally resolved (Wheeler et al.,  
455 2019). In conclusion, furrow ingression must require some rearrangement of the microtubule array. It  
456 is quite possible that an increase in  $\alpha$ -tubulin acetylation, as a consequence of ATAT-HA over-  
457 expression, somehow promotes the stabilization between kDNA and the basal body (which are also  
458 composed by MTs) thus impairing MTs rearrangements and cytokinesis. Basal body replication can be  
459 impaired in cells over-expressing ATAT-HA, since protozoa containing duplicated kDNA network, a  
460 single basal body and only one flagellum were observed. Unfortunately, we still do not know much  
461 about the cell cycle checkpoints of *T. cruzi* epimastigotes, what would enable a deeper discussion about  
462 the observed phenomenon.

463 A refringent button-like structure was visible by optic microscopy that started to grow in a time-  
464 dependent manner after induction of ATAT-HA over-expression with tetracycline. This round  
465 structure contains ATAT-HA, forming an insoluble and tridimensional structure that remains  
466 associated with isolated cytoskeletal and flagellar fractions. This atypical structure is electrodense  
467 and is observed by TEM most of the time in the anterior region, close to the nucleus and kinetoplast.  
468 It is not delimited by a membrane unit, which suggests that it could be a cumulus of protein, rich in  
469 *TcATAT*-HA, reminiscent to an inclusion body. Inclusion bodies are aggregates of misfolded protein  
470 known to occur in eucaryotic cells, for example during neurodegenerative disorders (Chung et al.,  
471 2018). Inclusion bodies are also found in bacteria as particles of aggregated protein (Singh and  
472 Panda, 2005). To our knowledge there are no reports of inclusion bodies in trypanosomatids  
473 occurring as a consequence of over-expression of exogenous proteins. It is also worth mentioning  
474 that we have use this over-expression systems for different proteins and never observed this  
475 phenotype (Ritagliati et al., 2015b, 2015a; Alonso et al., 2016; Tavernelli et al., 2019). We believe  
476 that these inclusion-body like structures are not occurring due to protein misfolding but as a  
477 consequence of the accumulation of ATAT-HA in a specific region the cytoskeleton. Suggestively,  
478 we also observe an accumulation of acetylated  $\alpha$ -tubulin around the kinetoplast and the inclusion  
479 body-like structure at the anterior region, where in normal conditions *TcATAT* is proposed to  
480 acetylate the microtubes as they polymerize. It is proposed that *T. cruzi* kinetoplast division is similar  
481 to that described to *Crithidia fasciculata* (Ferguson et al., 1994; Liu et al., 2005) and since the  
482 kinetoplast is part of the single mitochondrion, it is suggested that trypanosomatid's mitochondrion  
483 could start to segregate in the kinetoplast region (Ramos et al., 2011), which correlates with our  
484 observations. We propose that hyperacetylation impairs the division of the kDNA, given that the  
485 kinetoplast divides in coordination with the basal body. Cytoskeletal elements such as the flagellum,  
486 FAZ, flagellar pocket and the subpellicular microtubule array, all need to be duplicated and  
487 segregated in a coordinated manner in relation to the nuclear and kinetoplast cycles. The basal body  
488 in trypanosomes is the master organizer for the surrounding cytoskeleton, membranous structures,  
489 and organelles. Regulation of the basal body maturation, biogenesis, segregation and positioning is  
490 vital to ensure the shape and form of subsequent daughter cells (Elias et al., 2007). Further studies are  
491 required to determine the exact role of  $\alpha$ -tubulin acetylation in the division of the kinetoplast and the  
492 basal body.

## Tubulin hyperacetylation effect in *Trypanosoma cruzi*

493 Oliveira Santos et al, described the effect of Trichostatin A (TSA), a deacetylase inhibitor in *T. cruzi*.  
494 They report that one of the main effects of TSA treatment is  $\alpha$ -tubulin hyperacetylation, which  
495 induced microtubule cytoskeleton reorganization. They observed the presence of parasites with  
496 replicated kDNA, associated with basal bodies, but an incomplete cytokinesis. They also reported a  
497 higher number of protozoa in G2/M phase of the cell cycle and polynucleated cells with an aberrant  
498 phenotype (Santos et al., 2018). These results are similar to those observed in ATAT-HA over-  
499 expressing cells. Probably TSA treatment is targeting several deacetylases in *T. cruzi*, so it could  
500 promote the hyperacetylation of other proteins besides  $\alpha$ -tubulin, but the cytoskeletal remodeling  
501 seems to be linked to  $\alpha$ -tubulin acetylation.

502 Our study is the first report of the ATAT/MEC-17 homologue in trypanosomatids. Besides  
503 ATAT/MEC-17 itself, no other substrates than  $\alpha$ -tubulin have been reported for this family of lysine  
504 acetyltransferases to date. Mammalian ATAT has been shown to localize to the lumen of MTs, where  
505 it exerts its KAT activity *in vitro* (Szyk et al., 2014). *Tc*ATAT-HA tight association with MTs could  
506 also be due to the same luminal localization but this needs further corroboration. Our results suggest  
507 that a precise amount of acetylated/non-acetylated  $\alpha$ -tubulin is necessary for the correct kinetoplast  
508 division and assembly/disassembly of the basal body and the flagellum in epimastigotes. Further  
509 experiments are needed to determine the possible effect of  $\alpha$ -tubulin hyperacetylation over the other  
510 stages of *T. cruzi* life cycle.

### 511 5. Conflict of Interest

512 *The authors declare that the research was conducted in the absence of any commercial or financial*  
513 *relationships that could be construed as a potential conflict of interest.*

### 514 6. Author Contributions

515 Conceived and designed the experiments: VLA, MC, MCM, CSG, ES. Performed the experiments:  
516 VLA, MC, CSG, GMP, MEC, AP, LET. Wrote the manuscript: VLA, MCM and ES. All authors  
517 contributed with data analysis, share the responsibility related to the accuracy of the work, revised the  
518 manuscript, and approved its final version.

### 519 7. Funding

520 This work was supported by Agencia Nacional de Promoción Científica y Tecnológica, Ministerio de  
521 Ciencia, Tecnología e Innovación Productiva, Argentina [PICT 2017–1978], Universidad Nacional  
522 de Rosario [PIP 1BIO490] and Research Council United Kingdom [MR/P027989/1] and also by  
523 Conselho Nacional de Desenvolvimento Científico e Tecnológico (CNPq) and Fundação de Amparo  
à Pesquisa do Estado do Rio de Janeiro (FAPERJ).

### 525 8. Acknowledgments

526 We would like to thank Rodrigo Vena, Dolores Campos, Romina Manarin and Mara Ojeda for their  
527 technical assistance in confocal microscopy, cells and parasites culture and flow cytometry  
528 respectively. Also, we are grateful to Ariel Silver for the anti-PAR2 antibodies and Carla Ritagliati  
529 for the assistance with motility measurements using the CASA Hamilton equipment.

### 530 9. Reference

531 Akella, J. S., Wloga, D., Kim, J., Starostina, N. G., Lyons-Abbott, S., Morrisette, N. S., et al. (2010).  
532 MEC-17 is an  $\alpha$ -tubulin acetyltransferase. *Nature* 467, 218–222. doi:10.1038/nature09324.

## Tubulin hyperacetylation in *Trypanosoma cruzi*

533 Al-Bassam, J., and Corbett, K. D. (2012).  $\alpha$ -Tubulin acetylation from the inside out. *Proc. Natl. Acad. Sci.* 109, 19515–19516. doi:10.1073/pnas.1217594109.

534 Alonso, V. L., Ritagliati, C., Cribb, P., Cricco, J. A., and Serra, E. C. (2016). Overexpression of bromodomain factor 3 in *Trypanosoma cruzi* (TcBDF3) affects differentiation of the parasite and protects it against bromodomain inhibitors. *FEBS J.* 283, 2051–2066. doi:10.1111/febs.13719.

535 Alonso, V. L., Ritagliati, C., Cribb, P., and Serra, E. C. (2014a). Construction of three new gateway® expression plasmids for *Trypanosoma cruzi*. *Mem. Inst. Oswaldo Cruz* 109, 1081–1085. doi:10.1590/0074-0276140238.

536 Alonso, V. L., Villanova, G. V., Ritagliati, C., Motta, M. C. M., Cribb, P., and Serra, E. C. (2014b). *Trypanosoma cruzi* bromodomain factor 3 binds acetylated  $\alpha$ -tubulin and concentrates in the flagellum during metacyclogenesis. *Eukaryot. Cell* 13, 822–831. doi:10.1128/EC.00341-13.

537 Armon, A., Menon, K., O’Hara, A., MacDonald, L. M., Read, C. M., Sargent, K., et al. (2002). Efficacy of oryzalin and associated histological changes in Cryptosporidium-infected neonatal rats. *Parasitology* 125, 113–117. doi:10.1017/s003118200200197x.

538 Catta-Preta, C. M. C., Brum, F. L., da Silva, C. C., Zuma, A. A., Elias, M. C., de Souza, W., et al. (2015). Endosymbiosis in trypanosomatid protozoa: the bacterium division is controlled during the host cell cycle. *Front. Microbiol.* 6, 520. doi:10.3389/fmicb.2015.00520.

539 Chan, M. M. Y., Triemer, R. E., and Fong, D. (1991). Effect of the anti-microtubule drug oryzalin on growth and differentiation of the parasitic protozoan *Leishmania mexicana*. *Differentiation* 46, 15–21. doi:10.1111/j.1432-0436.1991.tb00861.x.

540 Chung, C. G., Lee, H., and Lee, S. B. (2018). Mechanisms of protein toxicity in neurodegenerative diseases. *Cell. Mol. Life Sci.* 75, 3159–3180. doi:10.1007/s00018-018-2854-4.

541 Coombes, C., Yamamoto, A., McClellan, M., Reid, T. A., Plooster, M., Luxton, G. W. G., et al. (2016). Mechanism of microtubule lumen entry for the  $\alpha$ -tubulin acetyltransferase enzyme  $\alpha$ TAT1. *Proc. Natl. Acad. Sci.* 113, E7176–E7184. doi:10.1073/pnas.1605397113.

542 Cueva, J. G., Hsin, J., Huang, K. C., and Goodman, M. B. (2012). Posttranslational acetylation of  $\alpha$ -tubulin constrains protofilament number in native microtubules. *Curr. Biol.* 22, 1066–1074. doi:10.1016/j.cub.2012.05.012.

543 Deng, W., Wang, C., Zhang, Y., Xu, Y., Zhang, S., Liu, Z., et al. (2016). GPS-PAIL: prediction of lysine acetyltransferase-specific modification sites from protein sequences. *Sci. Rep.* 6, 39787. doi:10.1038/srep39787.

544 Dostál, V., and Libusová, L. (2014). Microtubule drugs: Action, selectivity, and resistance across the kingdoms of life. *Protoplasma* 251, 991–1005. doi:10.1007/s00709-014-0633-0.

545 Elias, M. C., da Cunha, J. P. C., de Faria, F. P., Mortara, R. A., Freymüller, E., and Schenkman, S. (2007). Morphological Events during the *Trypanosoma cruzi* Cell Cycle. *Protist* 158, 147–157. doi:10.1016/j.protis.2006.10.002.

546 Eshun-Wilson, L., Zhang, R., Portran, D., Nachury, M., Toso, D., Lohr, T., et al. (2019). Effects of  $\alpha$ -tubulin acetylation on microtubule structure and stability. *Proc. Natl. Acad. Sci.*, 1–35. doi:10.1073/pnas.1900441116.

547 Ferguson, M. L., Torri, A. F., Pérez-Morga, D., Ward, D. C., and Englund, P. T. (1994). Kinetoplast DNA replication: mechanistic differences between *Trypanosoma brucei* and *Crithidia fasciculata*. *J. Cell Biol.* 126, 631–639. doi:10.1083/jcb.126.3.631.

548 Gadadhar, S., Bodakuntla, S., Natarajan, K., and Janke, C. (2017). The tubulin code at a glance. *J. Cell Sci.* 130, 1347–1353. doi:10.1242/jcs.199471.

549 Howes, S. C., Alushin, G. M., Shida, T., Nachury, M. V., and Nogales, E. (2013). Effects of tubulin acetylation and tubulin acetyltransferase binding on microtubule structure. *Mol. Biol. Cell* 25, 257–266. doi:10.1091/mbc.e13-07-0387.

550 Hubbert, C., Guardiola, A., Shao, R., Kawaguchi, Y., Ito, A., Nixon, A., et al. (2002). HDAC6 is a

## Tubulin hyperacetylation effect in *Trypanosoma cruzi*

582 microtubule-associated deacetylase. *Nature* 417, 455–458. doi:10.1038/417455a.

583 Kalebic, N., Martinez, C., Perlas, E., Hublitz, P., Bilbao-Cortes, D., Fiedorczuk, K., et al. (2012).  
584 Tubulin Acetyltransferase  $\alpha$ TAT1 Destabilizes Microtubules Independently of Its Acetylation  
585 Activity. *Mol. Cell. Biol.* 33, 1114–1123. doi:10.1128/mcb.01044-12.

586 Kaser, S., Warscheid, B., Chanfon, A., Ochsenreiter, T., Pusnik, M., Meisinger, C., et al. (2014).  
587 Trypanosomal TAC40 constitutes a novel subclass of mitochondrial-barrel proteins specialized  
588 in mitochondrial genome inheritance. *Proc. Natl. Acad. Sci.* 111, 7624–7629.  
589 doi:10.1073/pnas.1404854111.

590 Kull, F. J., and Sloboda, R. D. (2014). A slow dance for microtubule acetylation. *Cell* 157, 1255–  
591 1256. doi:10.1016/j.cell.2014.05.021.

592 L'Hernault, S. W., and Rosenbaum, J. L. (1985). Chlamydomonas alpha-tubulin is posttranslationally  
593 modified by acetylation on the epsilon-amino group of a lysine. *Biochemistry* 24, 473–478.  
594 doi:10.1021/bi00323a034.

595 Li, L., Wei, D., Wang, Q., Pan, J., Liu, R., Zhang, X., et al. (2012). MEC-17 deficiency leads to  
596 reduced  $\alpha$ -tubulin acetylation and impaired migration of cortical neurons. *J. Neurosci.* 32,  
597 12673–12683. doi:10.1523/JNEUROSCI.0016-12.2012.

598 Li, Y., Shah-Simpson, S., Okrah, K., Belew, A. T., Choi, J., Caradonna, K. L., et al. (2016).  
599 Transcriptome Remodeling in *Trypanosoma cruzi* and Human Cells during Intracellular  
600 Infection. *PLoS Pathog.* 12, e1005511. doi:10.1371/journal.ppat.1005511.

601 Liu, B., Liu, Y., Motyka, S. A., Agbo, E. E. C., and Englund, P. T. (2005). Fellowship of the rings:  
602 the replication of kinetoplast DNA. *Trends Parasitol.* 21, 363–369.  
603 doi:10.1016/j.pt.2005.06.008.

604 Makioka, A., Kumagai, M., Ohtomo, H., Kobayashi, S., and Takeuchi, T. (2000). Effect of the  
605 antitubulin drug oryzalin on the encystation of *Entamoeba invadens*. *Parasitol. Res.* 86, 625–  
606 629. doi:10.1007/pl00008542.

607 Miller, L. (2010). Image J band quantification.

608 Morejohn, L. C., Bureau, T. E., Molè-Bajer, J., Bajer, A. S., and Fosket, D. E. (1987). Oryzalin, a  
609 dinitroaniline herbicide, binds to plant tubulin and inhibits microtubule polymerization in vitro.  
610 *Planta* 172, 252–264. doi:10.1007/BF00394595.

611 Moretti, N. S., Cestari, I., Anupama, A., Stuart, K., and Schenkman, S. (2018). Comparative  
612 Proteomic Analysis of Lysine Acetylation in Trypanosomes. *J. Proteome Res.* 17, 374–385.  
613 doi:10.1021/acs.jproteome.7b00603.

614 Nakakura, T., Asano-Hoshino, A., Suzuki, T., Arisawa, K., Tanaka, H., Sekino, Y., et al. (2015). The  
615 elongation of primary cilia via the acetylation of  $\alpha$ -tubulin by the treatment with lithium chloride  
616 in human fibroblast KD cells. *Med. Mol. Morphol.* 48, 44–53. doi:10.1007/s00795-014-0076-x.

617 Nett, I. R. E., Martin, D. M. A., Miranda-Saavedra, D., Lamont, D., Barber, J. D., Mehlert, A., et al.  
618 (2009). The phosphoproteome of bloodstream form *Trypanosoma brucei*, causative agent of  
619 African sleeping sickness. *Mol. Cell. Proteomics* 8, 1527–1538. doi:10.1074/mcp.M800556-  
620 MCP200.

621 Piperno, G., LeDizet, M., and Chang, X. J. (1987). Microtubules containing acetylated alpha-tubulin  
622 in mammalian cells in culture. *J. Cell Biol.* 104, 289–302. doi:10.1083/jcb.104.2.289.

623 Portran, D., Schaedel, L., Xu, Z., Théry, M., and Nachury, M. V. (2017). Tubulin acetylation protects  
624 long-lived microtubules against mechanical ageing. *Nat. Cell Biol.* 19, 391–398.  
625 doi:10.1038/ncb3481.

626 Price, H. P., Peltan, A., Stark, M., and Smith, D. F. (2010). The small GTPase ARL2 is required for  
627 cytokinesis in *Trypanosoma brucei*. *Mol. Biochem. Parasitol.* 173, 123–131.  
628 doi:10.1016/j.molbiopara.2010.05.016.

629 Ramos, T. C. P., Freymüller-Haapalainen, E., and Schenkman, S. (2011). Three-dimensional  
630 reconstruction of *Trypanosoma cruzi* epimastigotes and organelle distribution along the cell

## Tubulin hyperacetylation in *Trypanosoma cruzi*

631 division cycle. *Cytom. Part A* 79 A, 538–544. doi:10.1002/cyto.a.21077.

632 Ritagliati, C., Alonso, V. L., Manarin, R., Cribb, P., and Serra, E. C. (2015a). Overexpression of  
633 Cytoplasmic TcSIR2RP1 and Mitochondrial TcSIR2RP3 Impacts on *Trypanosoma cruzi*  
634 Growth and Cell Invasion. *PLoS Negl. Trop. Dis.* 9, 1–22. doi:10.1371/journal.pntd.0003725.

635 Ritagliati, C., Villanova, G. V., Alonso, V. L., Zuma, A., Cribb, P., Motta, M. C. M., et al. (2015b).  
636 Glycosomal bromodomain factor 1 from *Trypanosoma cruzi* enhances trypomastigote cell  
637 infection and intracellular amastigote growth. *Biochem. J.* 473, 73–85. doi:10.1042/bj20150986.

638 Rosenzweig, D., Smith, D., Myler, P. J., Olafson, R. W., and Zilberstein, D. (2008). Post-  
639 translational modification of cellular proteins during *Leishmania donovani* differentiation.  
640 *Proteomics* 8, 1843–1850. doi:10.1002/pmic.200701043.

641 Sanchez, A. D., and Feldman, J. L. (2017). Microtubule-organizing centers: from the centrosome to  
642 non-centrosomal sites. *Curr. Opin. Cell Biol.* 44, 93–101. doi:10.1016/j.ceb.2016.09.003.

643 Santos, de O., Zuma, A. A., Francisca, N., da Cunha, J. P. C., de Souza, W., and Motta, M. C. M.  
644 (2018). Trichostatin A induces *Trypanosoma cruzi* histone and tubulin acetylation: effects on  
645 cell division and microtubule cytoskeleton remodelling. *Parasitology*, 1–10.  
646 doi:10.1017/s0031182018001828.

647 Sasse, R., and Gull, K. (1988). Tubulin post-translational modifications and the construction of  
648 microtubular organelles in *Trypanosoma brucei*. *J. Cell Sci.* 90 ( Pt 4), 577–89. Available at:  
649 <http://www.ncbi.nlm.nih.gov/pubmed/3075618>.

650 Schneider, A., Sherwin, T., Sasse, R., Russell, D. G., Gull, K., and Seebeck, T. (1987). Subpellicular  
651 and Flagellar Microtubules of *Trypanosoma brucei brucei* Contain the Same  $\alpha$ -Tubulin  
652 Isoforms. *J. Cell Biol.* 104, 431–438.

653 Shaw, M. K., Compton, H. L., Roos, D. S., and Tilney, L. G. (2000). Microtubules, but not actin  
654 filaments, drive daughter cell budding and cell division in *Toxoplasma gondii*. *J. Cell Sci.* 113,  
655 1241 LP – 1254. Available at: <http://jcs.biologists.org/content/113/7/1241.abstract>.

656 Shida, T., Cueva, J. G., Xu, Z., Goodman, M. B., and Nachury, M. V (2010). The major  $\alpha$ -tubulin K40  
657 acetyltransferase TAT1 promotes rapid ciliogenesis and efficient mechanosensation. *Proc. Natl.*  
658 *Acad. Sci.* 107, 21517–21522. doi:10.1073/pnas.1013728107.

659 Singh, S., and Panda, A. K. (2005). Solubilization and refolding of bacterial inclusion body proteins.  
660 *J. Biosci. Bioeng.* 99 4, 303–310.

661 Smircich, P., Eastman, G., Bispo, S., Duhagon, M. A., Guerra-Slompo, E. P., Garat, B., et al. (2015).  
662 Ribosome profiling reveals translation control as a key mechanism generating differential gene  
663 expression in *Trypanosoma cruzi*. *BMC Genomics* 16, 443. doi:10.1186/s12864-015-1563-8.

664 Souto-Padron, T., Cunha e Silva, N. L., and de Souza, W. (1993). Acetylated alpha-tubulin in  
665 *Trypanosoma cruzi*: immunocytochemical localization. *Mem. Inst. Oswaldo Cruz* 88, 517–528.  
666 doi:10.1590/S0074-02761993000400004.

667 Stargell, L. A., Heruth, D. P., Gaertig, J., and Gorovsky, M. A. (1992). Drugs affecting microtubule  
668 dynamics increase alpha-tubulin mRNA accumulation via transcription in *Tetrahymena*  
669 *thermophila*. *Mol. Cell. Biol.* 12, 1443–1450. doi:10.1128/mcb.12.4.1443.

670 Stokkermans, T. J. W., Schwartzman, J. D., Keenan, K., Morrisette, N. S., Tilney, L. G., and Roos,  
671 D. S. (1996). Inhibition of *Toxoplasma gondii* replication by dinitroaniline herbicides. *Exp.*  
672 *Parasitol.* 84, 355–370. doi:10.1006/expr.1996.0124.

673 Szyk, A., Deaconescu, A. M., Spector, J., Goodman, B., Valenstein, M. L., Ziolkowska, N. E., et al.  
674 (2014). Molecular basis for age-dependent microtubule acetylation by tubulin acetyltransferase.  
675 *Cell* 157, 1405–1415. doi:10.1016/j.cell.2014.03.061.

676 Tavernelli, L. E., Motta, M. C. M., Gonçalves, C. S., da Silva, M. S., Elias, M. C., Alonso, V. L., et  
677 al. (2019). Overexpression of *Trypanosoma cruzi* High Mobility Group B protein (TcHMGB)  
678 alters the nuclear structure, impairs cytokinesis and reduces the parasite infectivity. *Sci. Rep.* 9,  
679 1–16. doi:10.1038/s41598-018-36718-0.

## Tubulin hyperacetylation effect in *Trypanosoma cruzi*

680 Taylor, M. C., and Kelly, J. M. (2006). pTcINDEX: A stable tetracycline-regulated expression vector  
681 for *Trypanosoma cruzi*. *BMC Biotechnol.* 6, 1–18. doi:10.1186/1472-6750-6-32.

682 Traub-Cseko, Y. M., Ramalho-Ortigão, J. M., Dantas, A. P., de Castro, S. L., Barbosa, H. S., and  
683 Downing, K. H. (2002). Dinitroaniline herbicides against protozoan parasites: the case of  
684 *Trypanosoma cruzi*. *Trends Parasitol.* 17, 136–141. doi:10.1016/s1471-4922(00)01834-1.

685 Tsigankov, P., Gherardini, P. F., Helmer-Citterich, M., Späth, G. F., and Zilberstein, D. (2013).  
686 Phosphoproteomic analysis of differentiating *Leishmania* parasites reveals a unique stage-  
687 specific phosphorylation motif. *J. Proteome Res.* 12, 3405–3412. doi:10.1021/pr4002492.

688 Varberg, J. M., Padgett, L. R., Arrizabalaga, G., and Sullivan, W. J. (2015). TgATAT-Mediated  
689 alpha-Tubulin Acetylation Is Required for Division of the Protozoan Parasite *Toxoplasma*  
690 *gondii*. *mSphere* 1, 1–16. doi:10.1128/mSphere.00088-15. Editor.

691 Vidal, J. C., Souza, W. de, Vidal Cunha, J., and de Souza, W. (2017). Morphological and Functional  
692 Aspects of Cytoskeleton of Trypanosomatids. *Cytoskelet. - Struct. Dyn. Dis.*, 55–72.  
693 doi:<http://dx.doi.org/10.5772/57353>.

694 Wheeler, R. J., Gull, K., and Sunter, J. D. (2019). Coordination of the Cell Cycle in Trypanosomes.  
695 *Annu. Rev. Microbiol.* 73, 133–154.

696 WHO (2012). Research priorities for Chagas disease, human African trypanosomiasis and  
697 leishmaniasis. World Health Organization technical report series. v–xii, 1–100. Available at:  
698 <http://www.ncbi.nlm.nih.gov/pubmed/23484340>.

699 Zhou, H., Cheng, X., Xu, X., Jiang, T., Zhou, H., Sheng, Q., et al. (2018). Cloning, expression  
700 profiling, and acetylation identification of alpha-tubulin N-acetyltransferase 1 from *Bombyx*  
701 *mori*. *Arch. Insect Biochem. Physiol.* 98, 1–10. doi:10.1002/arch.21463.

702 Zhou, Q., and Li, Z. (2015). The  $\gamma$ -tubulin complex in *Trypanosoma brucei*: molecular composition,  
703 subunit interdependence and requirement for axonemal central pair protein assembly. *Mol.*  
704 *Microbiol.* 98, 667–680. doi:10.1007/s11065-015-9294-9. Functional.

705

## 706 10. Tables

707 Table I: Dm28c pTcINDEX ATAT-HA relative growth in the absence and presence of 200 mM  
708 Oryzalin for 72 hours. \*\* p<0.05 (t-student's test).

Dm28c pTcINDEX ATAT-HA relative growth	Tet -	Tet +
Without drug	100%	100%
200 mM Oryzalin	69%	85% (**)

709

## 710 11. Figure Captions

711 **Figure 1: The GCN5 acetyltransferase domain is conserved in *T. cruzi*.** (A) Schematic  
712 representation of ATAT/Mec17 form different organisms (in order: *T. cruzi*, *Plasmodium falciparum*,  
713 *Toxoplasma gondii*, *Tetrahymena thermophila*, *Caenorhabditis elegans*, *Homo sapiens*). The  
714 acetyltransferase domain is represented as light blue rectangles. (B) Multiple sequence alignment of  
715 the acetyltransferase domain using T-coffee and colored with Boxshade. Two conserved residues  
716 important for catalysis in *HsATAT* are marked with asterisks. **TcATAT is expressed in all life cycle**  
717 **stages of *T. cruzi*.** (C) Immunolocalization of *TcATAT* in Dm28c epimastigotes, amastigotes and  
718 trypomastigotes using rabbit polyclonal anti-*TcATAT* antibodies. Bar: 10  $\mu$ m. DAPI was used as  
719 nucleus and kinetoplast marker. The light blue arrow indicates the kinetoplast and the pink arrow

## Tubulin hyperacetylation in *Trypanosoma cruzi*

720 indicates the nucleus. **(D)** Total extracts of Dm28c epimastigotes (E), trypomastigotes (T) and  
721 amastigotes (A) were separated by SDS/PAGE and stained with Coomassie Blue (left panel),  
722 followed by western blot analysis using rabbit monoclonal anti-*Tc*ATAT antibodies (right panel).  
723

724 **Figure 2: Over-expression of ATAT-HA in epimastigotes increases  $\alpha$ -tubulin acetylation.** **(A)**  
725 Immunolocalization of ATAT-HA with rat monoclonal anti-HA antibodies in Dm28c p*Tc*INDEX-  
726 GW ATAT-HA epimastigotes induced with 0.5  $\mu$ g/ml tetracycline for 24 h. Bar: 5  $\mu$ m. DAPI was  
727 used as nucleus and kinetoplast marker. The light blue arrow indicates the kinetoplast and the pink  
728 arrow indicates the nucleus. **(B)** Total extracts of p*Tc*INDEX-GW ATAT-HA epimastigotes in the  
729 absence (-) or presence (+) of 0.5  $\mu$ g/ml tetracycline for 24 h were separated by SDS/PAGE and  
730 stained with Coomassie Blue (left panel), followed by western blot analysis using rat monoclonal  
731 anti-HA antibodies (right panel). **(C)** Western blot of total extracts of p*Tc*INDEX-GW ATAT-HA  
732 epimastigotes with 0.5  $\mu$ g/ml tetracycline at different time points post-induction using rat monoclonal  
733 anti-HA, mouse monoclonal anti-acetylated  $\alpha$ -tubulin (anti-AcTub), rabbit monoclonal anti-*Tc*ATAT  
734 antibodies and mouse monoclonal anti- $\alpha$ -tubulin (anti-  $\alpha$ Tub). Bands were quantified by  
735 densitometry using  $\alpha$ -tubulin signal to normalize the amount of ATAT-HA and acetylated  $\alpha$ -tubulin  
736 (right panel). **(D)** ATAT-HA autoacetylation assay. ATAT-HA was purified from *T. cruzi*  
737 epimastigotes and incubated in the absence (-) and presence (+) of AcetylCoA and then separated by  
738 SDS/PAGE followed by western blot analysis with rat monoclonal anti-HA antibodies and rabbit  
739 monoclonal anti-Acetylated Lysine (anti-AcLys).  
740

741 **Figure 3: ATAT-HA colocalizes with acetylated  $\alpha$ -tubulin in the cytoskeleton and flagella of**  
742 **epimastigotes.** **(A)** Immunolocalization of ATAT-HA with rat monoclonal anti-HA antibodies and  
743 mouse monoclonal anti-acetylated  $\alpha$ -tubulin (anti-AcTub) in isolated cytoskeletons and flagella of  
744 Dm28c p*Tc*INDEX-GW ATAT-HA epimastigotes induced with 0.5  $\mu$ g/ml tetracycline for 24 h. **(B)**  
745 Extracts enriched in cytoskeletal and flagellar proteins were analyzed by western blot with rat  
746 monoclonal anti-HA antibodies, rabbit polyclonal anti-*Tc*ATAT antibodies, mouse monoclonal anti-  
747 acetylated  $\alpha$ -tubulin (anti-AcTub) and anti  $\alpha$ -tubulin (anti-  $\alpha$ Tub). SN1, soluble protein extracts;  
748 SN2, soluble cytoskeletal and flagellar protein extracts; P, insoluble cytoskeletal and flagellar protein  
749 extracts.  
750

751 **Figure 4: Over-expression of ATAT-HA induced the formation of an inclusion body-like**  
752 **structure.** **(A)** Immunolocalization of ATAT-HA with rat monoclonal anti-HA antibodies in Dm28c  
753 p*Tc*INDEX-GW ATAT-HA epimastigotes induced with 0.5 mg/ml tetracycline at different time  
754 points p.i. The yellow arrow indicates the inclusion body-like structure, the light blue arrow indicates  
755 the kinetoplast and the pink arrow indicates the nucleus. DAPI was used as nucleus and kinetoplast  
756 marker. Bar: 5  $\mu$ m. **(B)** Transmission Electron Microscopy of Dm28c p*Tc*INDEX-GW ATAT-HA  
757 epimastigotes induced with 0.5  $\mu$ g/ml tetracycline for 48 h. ib-lk, inclusion body-like structure. This  
758 structure was seen in close proximity with the endoplasmic reticulum (fig. a, arrows) and was  
759 positioned close to the nucleus (n) and the kinetoplast (k) in the posterior part of the cell body (fig. b)  
760 or more commonly at the anterior end, close to the kinetoplast and the basal body (fig. c). The  
761 inclusions body is not surrounded by a membrane unit (fig. d). bb, basal body; f, flagellum. Bar: 1  
762  $\mu$ m.  
763

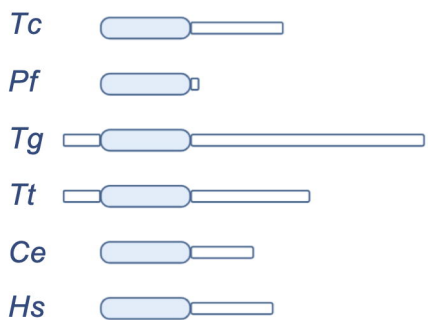
764 **Figure 5: ATAT-HA over-expression negatively impacts on epimastigotes growth.** **(A)** Growth  
765 curve of Dm28c p*Tc*INDEX-GW ATAT-HA epimastigotes in the absence (grey circles) and presence  
766 (green squares) of 0.5  $\mu$ g/ml tetracycline for 9 days. \*\*  $p < 0.005$ , \*\*\*  $p < 0.001$  (Student's t-test). **(B)**  
767 Immunolocalization of *Tc*ATAT, in Dm28c p*Tc*INDEX-GW ATAT-HA epimastigotes in the

## Tubulin hyperacetylation effect in *Trypanosoma cruzi*

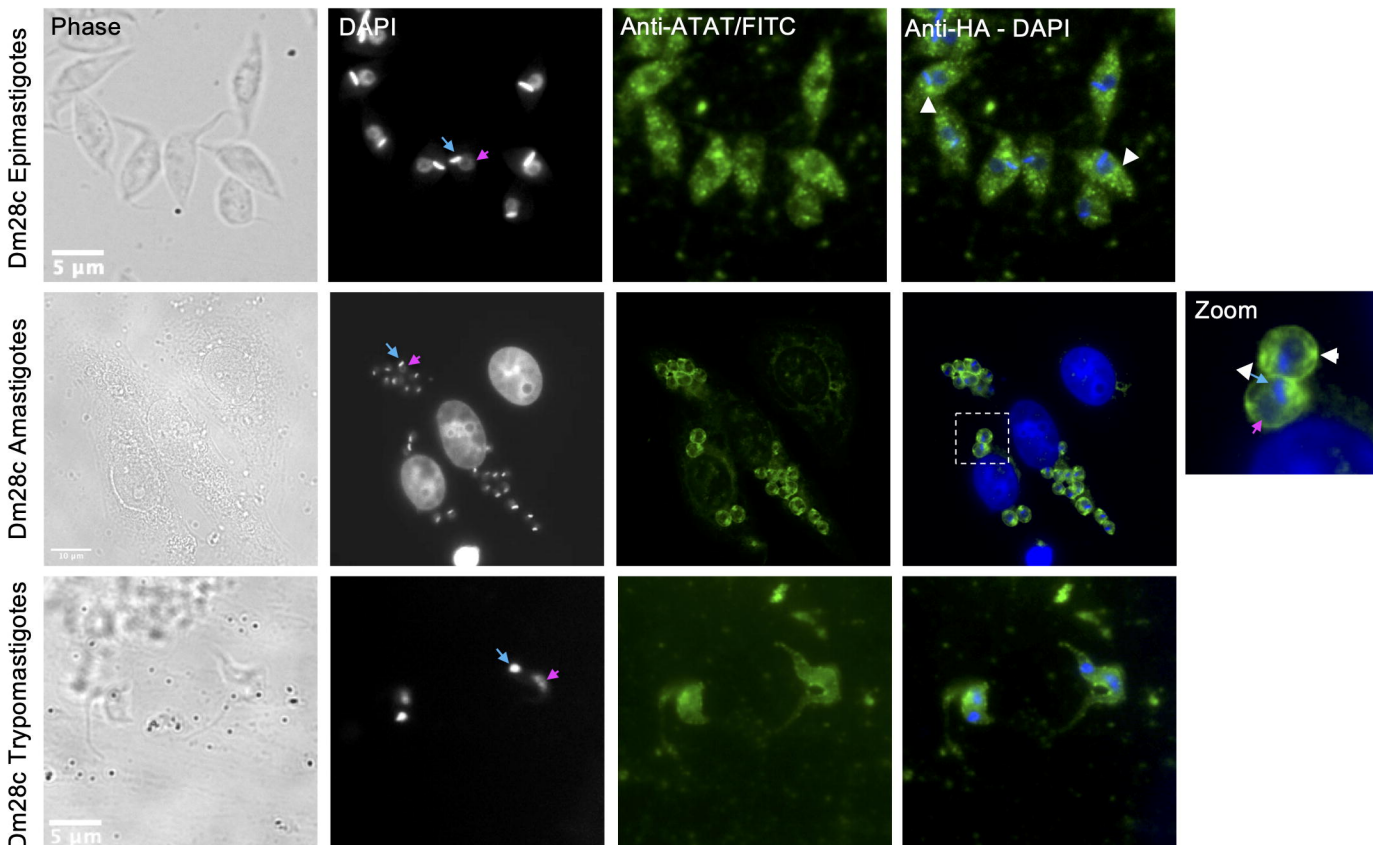
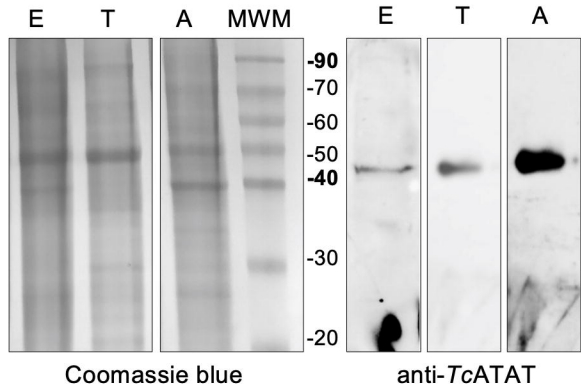
768 absence and presence of 0.5 µg/ml tetracycline for 24 and 48 h. Bar: 5 µm. DAPI was used as  
769 nucleus and kinetoplast marker. The light blue arrow indicates the kinetoplast and the pink arrow  
770 indicates the nucleus. Yellow arrowheads indicate parasites with an aberrant DNA content.  
771

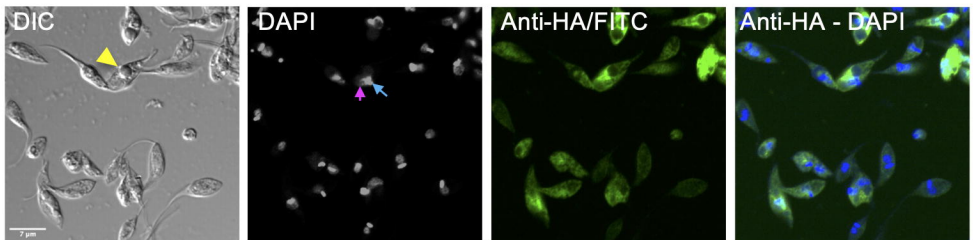
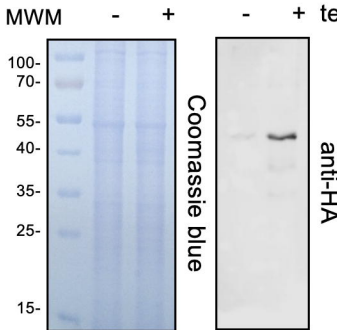
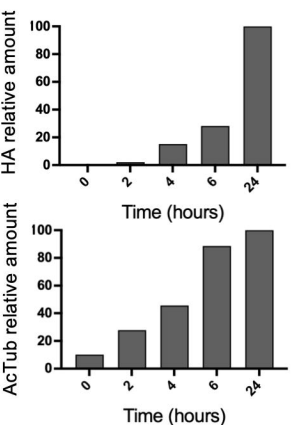
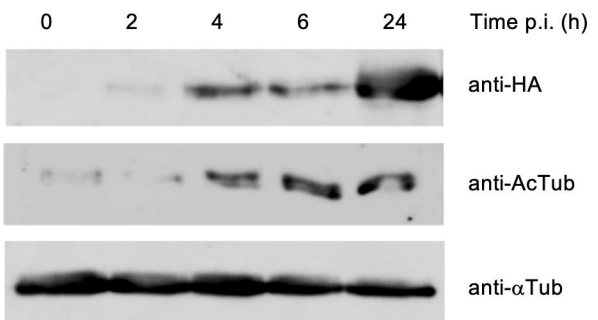
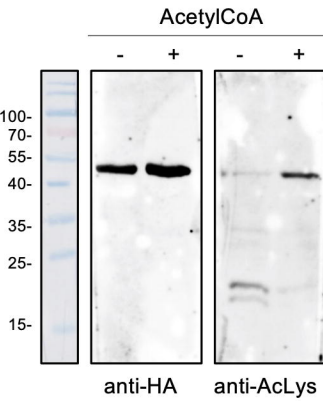
772 **Figure 6: Hyperacetylation alters the cell cycle progression.** (A) Flow cytometry analysis of  
773 synchronized Dm28c pTcINDEX-GW ATAT-HA epimastigotes in the absences (grey) and presence  
774 (green) of 0.5 µg/ml tetracycline at different time points. Histograms are plotted as the normalized  
775 number of events vs. propidium iodide absorbance (PI-A). (B) Bar graph with the percentages of  
776 cells in the different phases of the cell cycle. \*\*p < 0.005, \*\*\*p < 0.001 (Student's t test). (C) Images  
777 obtained by Scanning Electron Microscopy (SEM) of Dm28c pTcINDEX-GW ATAT-HA.  
778 Uninduced epimastigotes (TAT-) (figs. a-c). Parasites induced with 0.5 µg/ml tetracycline for 24 h  
779 (TAT+) (figs. d-i). Induced cells presented a phenotype that indicates cytokinesis arrest (figs. d-e,  
780 arrows) and the interruption in the progression of the cleavage furrow (figs. f-i, white arrows).  
781

782 **Figure 7: Over-expression TcATAT-HA causes phenotypic alterations in acetylated α-tubulin**  
783 **distribution and on mitochondrion ultrastructure of epimastigotes.** (A) Immunolocalization of  
784 ATAT-HA with rat monoclonal anti-HA antibodies and mouse monoclonal anti-acetylated α-tubulin  
785 (anti-AcTub) of Dm28c pTcINDEX-GW ATAT-HA epimastigotes induced with 0.5 µg/ml  
786 tetracycline for 24 h. Bar: 5 µm. DAPI was used as nucleus and kinetoplast marker. The light blue  
787 arrow indicates the kinetoplast and the pink arrow indicates the nucleus. Yellow arrowheads indicate  
788 accumulation of acetylated α-tubulin around the kinetoplast and the white arrowhead indicates  
789 accumulation of acetylated α-tubulin around the inclusion body-like structure. (B) Transmission  
790 Electron Microscopy of Dm28c pTcINDEX-GW ATAT-HA epimastigotes induced with 0.5 µg/ml  
791 tetracycline for 48 h. Parasites presented alterations in the mitochondrial branches and at the  
792 kinetoplast region, especially cristae swelling (figs. a and b, white arrows). Parasites presenting a  
793 kinetoplast with multiple and electrodense networks were also observed (fig. c) f, flagellum; k,  
794 kinetoplast; m, mitochondria; n, nucleus. Bar: 1 µm. (C) Transmission Electron Microscopy of  
795 Dm28c pTcINDEX-GW ATAT-HA. In uninduced epimastigotes the replicated kDNA is contained in  
796 a kinetoplast associated to two basal bodies (fig. a, black arrowheads). Epimastigotes induced with  
797 0.5 µg/ml tetracycline for 48 h presented atypical characteristics (figs. b-f). In this case, the replicated  
798 kDNA is contained in a kinetoplast associated to a single basal body (fig. b, black arrowhead), which  
799 result is kinetoplast division impairment in a cell with two nuclei. The kinetoplast region is  
800 continuous with mitochondrial branches (fig. c, black arrows). The kDNA replication occurs during  
801 the S phase when the antipodal sites contain proteins involved in this process (fig. d, black arrows).  
802 Since the kDNA replicates, but the kinetoplast does not divide, the network curves and folds over  
803 itself, becoming round and presenting an atypical topology. The kinetoplast shape also changes its  
804 format from disk to round (figs. d-f). f, flagellum; k, kinetoplast; n, nucleus. Bars = 1 µm (a and b),  
805 200 nm (c-f). (D) Dm28c pTcINDEX-GW ATAT-HA epimastigotes induced with 0.5 µg/ml  
806 tetracycline for 48 h and stained with Mitotracker CMTMRos. DAPI was used as nucleus and  
807 kinetoplast marker. The light blue arrow indicates the kinetoplast and the pink arrow indicates the  
808 nucleus. The upper panel shows a parasite with a kinetoplast containing a duplicated kDNA and two  
809 nuclei, while the lower panel shows a  
810

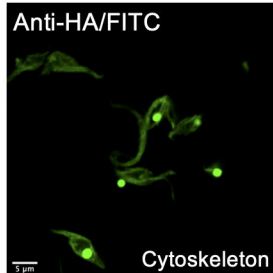
**A****B**

TcATAT	78	YVLLCQ-----DGYGV <b>C</b> ILKMGVK <b>K</b> I <b>F</b> VTHPSYSSLVEIDPLCV <b>L</b> DFFVDT <b>S</b> QRK <b>G</b>
PfATAT	65	IYCLIH-----TDGLIG <b>F</b> KIK <b>G</b> EKNLY <b>D</b> KI-K-LHY <b>G</b> KCT <b>C</b> V <b>L</b> D <b>F</b> Y <b>I</b> LE <b>F</b> Q <b>K</b> R <b>G</b>
TgATAT	232	LFLRVN-----KGVL <b>S</b> FLIK <b>T</b> GP <b>K</b> LI <b>W</b> IGNSS-G-MERINAL <b>S</b> LD <b>F</b> Y <b>V</b> LES <b>C</b> ORE <b>G</b> H
TtMec17	72	VYIVAE-----GRT <b>C</b> Q <b>F</b> IK <b>V</b> G <b>K</b> N <b>I</b> F <b>Y</b> R <b>D</b> MM-G <b>N</b> IK <b>E</b> I <b>K</b> P <b>L</b> C <b>V</b> L <b>D</b> F <b>V</b> H <b>E</b> S <b>C</b> Q <b>R</b> Q <b>C</b> Y
CeATAT2	65	LYLSWK-YDEEK <b>V</b> S <b>R</b> LM <b>G</b> FA <b>K</b> V <b>G</b> R <b>K</b> I <b>F</b> LY <b>D</b> SQ-M <b>Q</b> TY <b>E</b> GE <b>I</b> L <b>C</b> LL <b>D</b> F <b>V</b> H <b>F</b> S <b>C</b> Q <b>R</b> Q <b>G</b> V
HsMec17	77	VYILKDSSARPAGKGAI <b>I</b> <b>G</b> FI <b>K</b> V <b>G</b> Y <b>K</b> I <b>F</b> VL <b>D</b> DR-EAH <b>N</b> EV <b>E</b> PL <b>C</b> I <b>L</b> D <b>F</b> Y <b>I</b> HE <b>S</b> V <b>Q</b> R <b>H</b> G

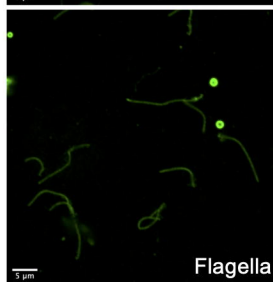
**C****D**

**A****B****C****D**

**A** Anti-HA/FITC

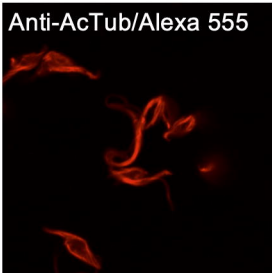


Cytoskeleton

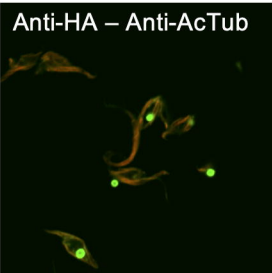


Flagella

Anti-AcTub/Alexa 555



Anti-HA – Anti-AcTub



**B**

- Tet

SN1 SN2 P



Anti-HA



Anti-AcTub



Anti-ATAT



Anti- $\alpha$ Tub

+ Tet

SN1 SN2 P



Anti-HA



Anti-AcTub



Anti-ATAT



Anti- $\alpha$ Tub

